

Modulators Selectively Reshape α -Synuclein Phase Transitions

Holly Masson^{1,2,3}, Massimiliano Paesani^{1,2,3}, and Ioana M. Ilie^{1,2,3*}

¹ Van 't Hoff Institute for Molecular Sciences, University of Amsterdam, Amsterdam, The Netherlands

² Amsterdam Center for Multiscale Modeling (ACMM), University of Amsterdam, the Netherlands

³ Computational Soft Matter (CSM), University of Amsterdam, the Netherlands

(*Corresponding author: i.m.ilie@uva.nl)

Protein phase transitions govern numerous diseases, including neurodegenerative disorders such as Parkinson's and Alzheimer's. In Parkinson's disease, distinct species of the protein α -synuclein undergo phase transitions from highly disordered to ordered β -rich states. The emerging species and transitions between them can be reshaped by chaperones, small molecules, peptides or antibodies. Here, we use coarse-grained simulations to understand the effect of modulators on the thermodynamics and kinetics of α -synuclein transformations and phase transitions. Each protein is represented as a single morphing particle that transforms from a soft sphere (disordered state) to a hard spherocylinder (β -rich state), while modulators are modeled as soft isotropic particles mimicking small peptides. The results show that purely repulsive modulators do not alter the final outcome, *i.e.*, fibrils form following the same mechanisms independently of the modulator concentration. Attractive interactions towards the disordered protein slow down fibril formation in a dose-dependent manner by stabilizing intermediate species, and strong attraction yields persistent disordered heteroclusters. In contrast, specific attraction to the β -rich state results in shorter fibrils through direct modulator surface "capping" that introduce kinetic barriers to monomer templating at the fibril ends and inhibit lateral attachment. Together, these results link modulator properties and environmental conditions to the effects on nucleation, fibril elongation and off-pathway trapping, providing a quantitative roadmap for selecting modulator properties and strategies that redirect phase transitions toward desirable endpoints. Additionally, they provide guiding principles for the development of intervention strategies and the engineering of novel materials with tunable and responsive properties.

I. INTRODUCTION

Parkinson's disease is the second most common neurodegenerative disorder, estimated to affect almost 2% of people over the age of 65, with prevalence expected to increase as populations age [1, 2]. A hallmark of this disease is the presence of intracellular protein accumulations known as Lewy inclusions in the brain of diseased patients. These inclusions can be either spherical ('Lewy body') or rod-shaped ('Lewy neurite'), and are composed of distinct species of the protein α -synuclein (α -syn) [2, 3]. These are found in the dopamine-producing neurons of the brain, where they contribute to dopamine loss and thereby to the onset of the characteristic motor symptoms of the disease [2]. In the years since its association with Parkinson's disease was established in the late 1990s, α -syn has become a focal point in the study of this disease, particularly the kinetics and thermodynamics associated with pathological phase transitions and the factors that influence them [3–5].

α -syn is a 140-aminoacid intrinsically disordered protein, which is highly abundant in the brain, localized primarily at presynaptic terminals [6]. In its native soluble state, α -syn lacks a prevalent secondary structure, is highly dynamic and can adopt different conformations depending on its environment [6–8]. For instance, it is known to curl into α -helical conformations against membranes or detergent micelles, and to adopt β -sheets when it self-assembles into amyloid fibrils, such as those found in Parkinson's disease Lewy inclusions [7]. The central segment of the protein, the non-amyloid component is particularly prone to β -sheet formation, and thus of great interest in the study of α -syn phase transitions and aggregation [9].

Aggregation typically proceeds via a nucleation-dependent mechanism involving three kinetic stages: a lag phase, in which critical nuclei form; an elongation phase, during which fibrils rapidly grow via different mechanisms (monomer addition, fibril breakage, secondary nucleation); and a saturation phase, in which monomer depletion leads to a steady-state [10, 11]. During the lag phase a series of species emerge, *i.e.*, soluble (liquid-like) oligomers and protofibrils, some of which evolve into insoluble highly ordered fibrillar structures with a characteristic cross- β -sheet architecture [7, 12]. While fibrils are the dominant component of Lewy inclusions, oligomeric species are increasingly recognized as also being able of disrupting lipid membranes and interfering with intracellular processes [13, 14]. The formation of fibrillar structures can occur following two distinct mechanisms, *i.e.*, a homogeneous mechanism, where monomers self-associate (known as primary nucleation), or a heterogeneous mechanism involving a separate surface (for example, a pre-existing fibril or lipid membrane; known as secondary nucleation), which lowers the energy barrier for nucleus formation [15, 16]. Primary nucleation itself can proceed either in one-step (1SN) in which two monomers meet and bind to each other in a single thermodynamic event, or via a two-step (2SN) mechanism, wherein a disordered (often liquid-like) intermediate is involved to catalyze the formation of fibrillar species [17]. Recent studies indicate that fragmentation of a fibril can also accelerate fibrillization, due to providing new fibril ends where polymerisation can occur [14, 18]. This raises important questions about the optimal approach for intervention during the early stages of Parkinson's disease, as breaking down the fibrils may simply exacerbate the problem. The key, it would seem, lies with modulation of the emerging species and transitions between them.

Small molecules, peptides and antibodies have all shown promise as modulators of aggregation *in vitro* and in cellular models [19–22]. However, the intrinsically disordered nature of α -synuclein, and the structural heterogeneity of the emerging species, pose substantial challenges for drug discovery, particularly in identifying stable binding sites or predicting consistent structural responses to small molecules [2, 5, 20, 23]. Given these challenges in designing modulators experimentally, computational methods have emerged as valuable tools to explore the aggregation pathway [17, 24, 25]. For instance, by integrating atomistic molecular dynamics simulations with machine-learning analysis, two promising small molecules able of modulating the interaction between α -synuclein and its partner protein 14-3-3 ζ were identified [26]. One, Var84, acts as an orthosteric ligand that likely binds at the α -syn recognition site and directly competes for binding, while the other, DB11581, functions as an allosteric ligand that influences the interaction indirectly through binding at a remote site on 14-3-3 ζ . Long atomistic molecular dynamics simulations showed that the small molecule fasudil preferentially binds to the C-terminal region of α -synuclein through a combination of charge–charge and aromatic π -stacking interactions, while dynamically shuttling among transient binding modes rather than forming multiple stable contacts. [27]. Rationally redesigned peptides targeting the fibril surface of α -synuclein were developed through computational mutagenesis and docking, and later on were shown to effectively suppress fibril and oligomer formation *in vitro* while reducing α -syn-induced toxicity in cellular models [28].

While atomistic simulations are effective at the monomeric level or for small aggregates, coarse-grained simulations are particularly well suited for gaining insight into effects of small agents on α -syn phase separation, nucleation, fibrilization or crowding, where the processes occur on long timescales and involve large, structurally diverse assemblies [17, 29, 30]. Coarse-grained simulations of α -synuclein in crowded environments (employing the Martini3 force field) revealed that the protein is highly sensitive to its local environmental context. Specifically, in crowded conditions, α -syn self-assembly is driven primarily by entropic effects that promote condensate formation, whereas high-salt environments stabilize aggregation through enthalpic interactions that modify chain organization and intermolecular contacts [31]. One-residue coarse-grained models like CALVADOS [32] revealed that polyethylene glycol-induced crowding responses depend on sequence charge patterning, highlighting the effects of cellular-like environments on α -synuclein compaction and its propensity for phase separation [33]. We developed a single-particle coarse-grained model for intrinsically disordered proteins, in which the protein is represented as a morphing particle that switches between two conformational states, *i.e.*, a disordered state modeled as a soft isotropic sphere and a β -rich state modeled as an elongated rod with directional interactions (Fig. 1) [12]. This model provided mechanistic insight into α -synuclein nucleation. Specifically, that α -synuclein nucleation can occur via either direct monomer-to-fibril conversion (one-step) or through metastable intermediates (two-step), with the dominant pathway determined by protein con-

centration and environmental conditions [12]. This model was later extended to represent each protein as a chain of morphing particles, enabling a more detailed investigation of α -synuclein fibrillar growth [34]. Specifically, free energy calculations revealed that an attaching protein becomes trapped in a misfolded state, thereby inhibiting fibrillar growth until it rearranges to adopt the fibril-growing conformation, consistent with experimental observations [35].

Here, we build upon the morphing-particle model to investigate how modulators influence α -synuclein species formation and phase transitions. We extend the model by introducing a new type of particle, a small soft sphere, that mimics the interaction of a peptide modulator with α -syn. By systematically tuning the interactions between the modulator and the disordered and β -rich proteins, we find that specific and nonspecific interactions selectively reshape the emerging α -synuclein species and their phase transitions. Specifically, nonspecific interactions with the disordered protein allow the modulator to act as a bridge between α -synuclein monomers, shifting the balance between one-step and two-step nucleation, thereby tuning the lag phase. This bridging leads to prolonged nucleation timescales and the formation of larger clusters composed predominantly of disordered α -syn and modulators. Specific interactions with the β -rich proteins influence fibril nucleation and elongation, giving rise to shorter fibrils, whose growth is prevented by the accumulation of modulators on their surfaces. This protected surface blocks the addition of free peptides and effectively inhibits further fibril elongation. Together, these distinct modes of modulation, *i.e.*, bridging of disordered monomers and selective binding to β -rich conformers, reshape the kinetics, morphology and stability of α -synuclein phase transitions and species. They provide quantitative insight into what modulator properties can be designed and tuned to control species formation and α -synuclein phase transitions.

II. COMPUTATIONAL METHODS

A. α -syn and modulator models

We build on a previously introduced model for the amyloidogenic core of α -syn, which successfully captured thermodynamic and kinetic properties of self-assembly, including the formation of oligomers and fibrils, as well as nucleation mechanisms [12]. This model captures the ability of the protein to be intrinsically disordered in solution and adapt to attain β -rich structures in fibrils. Hence, in the disordered state, α -syn is modeled as a soft sphere with isotropic interactions. In the folded state, the protein morphs to become a hard spherocylinder with anisotropic interactions, representing the highly directional contacts associated with β -sheet stacking (Fig. 1). Transitions between these states are governed by an internal coordinate λ for each particle and occur in response to the environment. In line with experimental findings, the disordered state is favored over the ordered state in solution. In the simulation, this is accounted for by introducing an internal potential, $\Phi_\lambda(\lambda)$, that favors disordered states for the

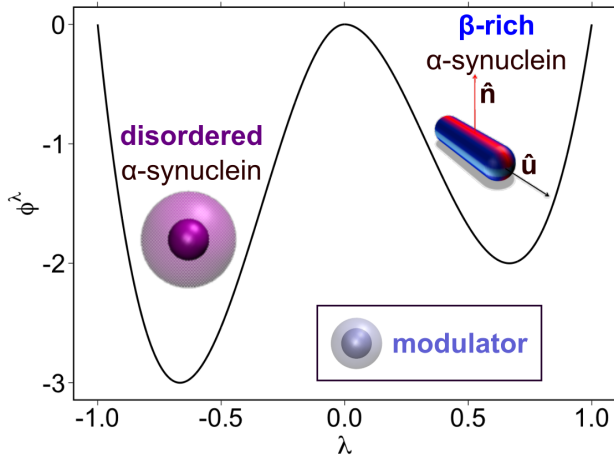


FIG. 1. The internal potential plotted against the internal coordinate for $\varepsilon_\lambda^S = 3$ and $\varepsilon_\lambda^R = 2$, see Eq. (1). Shown are representative snapshots of α -syn in the disordered state (purple sphere) and α -syn in the β -rich ordered state (blue spherocylinder with red patches). The inset shows the modulator (light blue sphere). Note that only the protein particles are morphing between disordered and ordered states according to λ , while the modulator's state remains unchanged.

free particles over ordered states for the β -rich fibril-bound particles. Hence, this potential is constructed from two third order polynomials that reach local minima of $-\varepsilon_\lambda^S$ and $-\varepsilon_\lambda^R$ for $\lambda = \pm \frac{2}{3}$, and are separated by a local maximum at $\lambda = 0$:

$$\Phi_\lambda(\lambda) = \begin{cases} -6.75 \varepsilon_\lambda^S (\lambda^2 + \lambda^3) & \text{for } \lambda < 0 \\ -6.75 \varepsilon_\lambda^R (\lambda^2 - \lambda^3) & \text{for } \lambda \geq 0. \end{cases} \quad (1)$$

The relative depth of each well, controlled by the parameters ε_λ^S and ε_λ^R (for sphere and rod, respectively), determines the intrinsic stability of each state in the absence of external interactions. As the value of λ_i changes, the properties of the particle are able to evolve continuously, endowing the particle with the ability to morph between states. Note that although the folded state is unfavourable in solution, it becomes the stable state in a fibril. This stability arises from the attractive interactions between proteins. In addition, internal states are linked to the geometrical properties of the particles via a smoothed step function defined as

$$\mu(\lambda) = \begin{cases} 0, & \lambda < -1, \\ \frac{\tanh(A_\mu \lambda)}{2 \tanh(A_\mu)} + \frac{1}{2}, & -1 \leq \lambda \leq 1, \\ 1, & \lambda > 1 \end{cases} \quad (2)$$

which ensures that shape changes occur only within a transition region of width A_μ . This then translates into the diameter $D(\lambda) = D_S + \mu(\lambda)(D_R - D_S)$ and length $L(\lambda) = L_S + \mu(\lambda)(L_R - L_S)$ of a particle, with the subscripts S and R denoting a sphere and a spherocylinder, respectively.

The current study introduces a third monomorphic ‘modulator’ particle to the model, capable of interacting with the protein. In contrast to the polymorphic α -syn particle, which

can dynamically transition between disordered and ordered states via an internal coordinate, the modulator particle introduced in this study is modelled as a single coarse-grained soft sphere, with a fixed diameter and fixed length.

B. Interaction potentials

Due to the polymorphism of the particles, the interaction between different α -syn-proteins is also described by an internal state-dependent potential. This is particularly important in a system such as this, where particles morph from soft isotropic spheres (representing a disordered protein) to hard anisotropic spherocylinders (representing a ordered protein), as the type and strength of steric interactions differ significantly between these two states. Since the particle’s conformation, and thus its effective shape and properties, vary continuously as a function of the internal coordinate λ_i , the interaction dynamically adapts to these changes.

The repulsion between any two particles i and j characterized by their center of mass positions, \mathbf{r}_i , \mathbf{r}_j , orientations, $\hat{\mathbf{u}}_i$, $\hat{\mathbf{u}}_j$, and internal states, λ_i, λ_j , is computed based on the minimum distance between their long axes $d_{\min}(\mathbf{r}_i, \mathbf{r}_j, \hat{\mathbf{u}}_i, \hat{\mathbf{u}}_j, \lambda_i, \lambda_j) = \min_{\alpha_i, \alpha_j} |(\mathbf{r}_i + \alpha_i \hat{\mathbf{u}}_i) - (\mathbf{r}_j + \alpha_j \hat{\mathbf{u}}_j)|$ [12, 34, 36]. Here, $\hat{\mathbf{u}}_i$ and $\hat{\mathbf{u}}_j$ are unit vectors pointing along the long axes of the particles and α_i and α_j are two minimization parameters obtained from $|\alpha_i| \leq \frac{1}{2}(L_i - D_i)$ and $|\alpha_j| \leq \frac{1}{2}(L_j - D_j)$, respectively.

The repulsive potential accounts for the softness of the particles, which depends on their internal state. As such, the repulsion between spherical particles is softer than between spherocylindrical ones, reflecting the looser packing of the protein in its disordered state compared to the more compact ordered state. Furthermore, the repulsive potential should become significant, *i.e.*, increase above the thermal energy $k_B T$ with k_B Boltzmann’s constant and T the temperature, when the minimum distance between two particles is shorter than the average of their radii, $\bar{D} = \frac{1}{2}(D_i + D_j)$. The repulsive potential between any two particles then reads

$$\frac{\Phi_{\text{rep}}^\lambda}{k_B T} = \begin{cases} \left(\frac{2\bar{D}}{d_{\min}} - 1 \right)^n & \text{for } d_{\min} < 2\bar{D} \\ 0 & \text{for } d_{\min} > 2\bar{D}, \end{cases} \quad (3)$$

where the exponent, *i.e.*, the hardness of the potential. This was selected to vary from 4 to 6 following $n = 4 + (\mu_i + \mu_j)$ for α -syn- α -syn interactions. For α -syn-modulator repulsion the exponent was set to 5 to reflect the structural compactness of a modulator, which is greater than that of a disordered protein, yet less tightly arranged than the folded conformation of α -syn.

The accumulation of the proteins is driven by attractive potentials, designed to reflect van der Waals, hydrophobic interactions and hydrogen bonding between the proteins. Importantly, the strength and character of these interactions depend on the distance and orientations between particles, and also on their conformational states. Disordered α -syn, owing to their larger radii of gyration and packing, interact via weaker,

longer-ranged and mostly isotropic forces. In contrast, folded β -rich proteins form compact, anisotropic structures where short-ranged, directional hydrogen bonding dominates, consistent with β -sheet stacking in fibrils. The modulators are modeled as isotropic particles, mimicking the structural compactness of a folded polypeptide domains. The proposed potential $\Phi_{\text{attr}} = \Phi_{\text{attr}}^{\lambda} + \Phi_{\text{attr}}^M$ encompasses the interactions between between α -syn proteins, $\Phi_{\text{attr}}^{\lambda}$, and interactions between the α -syn molecules and the modulator, Φ_{attr}^M .

The α -syn- α -syn potential, $\Phi_{\text{attr}}^{\lambda}$, is constructed as the sum of three contributions [34?],

$$\frac{\Phi_{\text{attr}}^{\lambda}}{k_B T} = \eta(d_{\min}) \left\{ \mathcal{C}_{\text{SS}} (1 - \mu_i) (1 - \mu_j) + \mathcal{F}_{\text{RR}} \mu_i \mu_j + \mathcal{C}_{\text{SR}} [\mu_i (1 - \mu_j) + \mu_j (1 - \mu_i)] \right\}, \quad (4)$$

each associated with a different type of interaction: disordered-disordered (sphere-sphere), governed by \mathcal{C}_{SS} , ordered-ordered (rod-rod), governed by \mathcal{F}_{RR} , and disordered-folded (sphere-rod), defined through \mathcal{C}_{SR} , pairs. This potential is scaled by a distance-dependent function, $\eta(d_{\min}) = \frac{\tanh(A_{\text{attr}}(d_{\min} - 2\bar{D}))}{\tanh(2A_{\text{attr}}\bar{D})}$, which ensures that the attraction turns off smoothly at the cut-off range $d_{\min} < 2\bar{D}$. The steepness of the transition between $\eta(0) = -1$ and $\eta(2\bar{D}) = 0$ is given by the parameter $A_{\text{attr}} = a_{\text{attr}}(\mu_i + \mu_j) + b_{\text{attr}}$, with $a_{\text{attr}} > 0$ and $b_{\text{attr}} > 0$. The potential in Eq. (4) reduces to a purely distance dependent attraction with a minimum at $-\mathcal{C}_{\text{SS}}$ for two spheres with $\mu_i \simeq \mu_j \simeq 0$.

The interaction between two rods with $\mu_i \simeq \mu_j \simeq 1$ is described by the second term on the r.h.s., with $\mathcal{F}_{\text{RR}} = [\mathcal{C}_{\text{RR}}^{\text{w}} + g_{ij} \mathcal{C}_{\text{RR}}^{\text{s}}]$ accounting also for the relative orientations of the ordered proteins. Here f_{ij} and g_{ij} are two directional functions that describe the parallel arrangement of the rods and their hydrogen bonding ability, respectively. The two constants $\mathcal{C}_{\text{RR}}^{\text{w}}$ and $\mathcal{C}_{\text{RR}}^{\text{s}}$ represent the weak van der Waals and hydrophobic interactions, and the strong hydrogen bonds between two proteins, respectively. Essentially, $f_{ij} \in [0, 1]$ is an alignment factor that accounts for the parallel alignment of two rods ($\hat{\mathbf{u}}_i \cdot \hat{\mathbf{u}}_j$)² and the sliding of the rods along their long axes $h(\hat{\mathbf{u}}_i \cdot \hat{\mathbf{r}}_{ij})h(\hat{\mathbf{u}}_j \cdot \hat{\mathbf{r}}_{ij})$ and is thus defined as $f_{ij} = (\hat{\mathbf{u}}_i \cdot \hat{\mathbf{u}}_j)^2 h(\hat{\mathbf{u}}_i \cdot \hat{\mathbf{r}}_{ij})h(\hat{\mathbf{u}}_j \cdot \hat{\mathbf{r}}_{ij})$. Here $h(x) = 1 - ax^2$ for $x^2 < 1/a$ and 0 otherwise captures the variations in energy as one rod is displaced along its long axis, at fixed orientation and d_{\min} . The interaction is the most favorable when the connecting vector \mathbf{r}_{ij} is perpendicular to both rods. The directional function $g_{ij} \in [0, 1]$ accounts for the hydrogen bonding ability between two proteins. This is achieved by endowing the particle with an orientation vector, $\hat{\mathbf{n}}$, perpendicular to the long axis $\hat{\mathbf{u}}_i$, and favoring its alignment in parallel to the center-to-center direction $\hat{\mathbf{r}}_{ij}$, resulting in $g_{ij} = (\hat{\mathbf{r}}_{ij} \cdot \hat{\mathbf{n}}_i)^p (\hat{\mathbf{r}}_{ij} \cdot \hat{\mathbf{n}}_j)^p$, with p an integer.

The attractive potential, Φ_{attr}^M , between modulator particles and α -syn particles is formulated in a simplified manner to represent isotropic interactions with both disordered and or-

dered α -syn:

$$\frac{\Phi_{\text{attr}}^M}{k_B T} = \theta(i, j) \eta(d_{\min}) \left\{ \mathcal{C}_{\text{MS}} (1 - \mu_i) (1 - \mu_j) + \mathcal{C}_{\text{MR}} [\mu_i (1 - \mu_j) + \mu_j (1 - \mu_i)] \right\}, \quad (5)$$

with $\theta(i, j)$ a step function that returns 1 of any of the two particles is a modulator and 0 otherwise. Modulators are modelled as uniform spheres, which do not change properties, and thus their internal state is fixed in the simulations to $\mu = 0$. Therefore, the attraction to the α -syn molecules is described by a distance dependent potential, which captures the binding abilities to disordered and ordered proteins. Similarly as for two α -syn proteins, the distances dependent function $\eta(d_{\min})$ will scale with the properties of the interacting protein. Since both terms on the r.h.s. of Eq. (5) scale with the average diameter of the interacting particles, the interaction between a modulator and a spherical particle, which has a minimum at \mathcal{C}_{MS} , is longer ranged than that between a modulator and an ordered particle, with a minimum at \mathcal{C}_{MR} .

III. BROWNIAN DYNAMICS SIMULATIONS

All simulations were carried out using Brownian dynamics to simulate the translational, rotational and internal dynamics of the particles. Here, we limit ourselves at presenting just the generalized equation of motion as the three independent equations have been previously introduced [12, 34, 37]. The generalized equation of motion is given by [38, 39]

$$\mathbf{Q}(t + \Delta t) - \mathbf{Q}(t) = -\mu^Q \frac{\partial \mathcal{A}}{\partial \mathbf{Q}} \Delta t + k_B T \frac{\partial}{\partial \mathbf{Q}} \cdot \mu^Q \Delta t + (\mu^Q)^{1/2} \Theta^Q(t) \sqrt{2k_B T \Delta t}, \quad (6)$$

where \mathbf{Q} represents the full set of generalised coordinates. The first term on the r.h.s. describes the displacements of \mathbf{Q} over a time-step Δt , arising from the balance between the thermodynamic force $\mathcal{F} = -\partial \mathcal{A} / \partial \mathbf{Q}$, where \mathcal{A} is the free energy as a function of \mathbf{Q} , and the opposing solvent friction, which is the inverse of the mobility matrix μ^Q . The second term accounts for inhomogeneity of the mobility tensor μ^Q , which leads to a non-zero contribution even in the absence of a deterministic force. The last term corresponds to Brownian displacements of the generalized coordinate. The components of the time-dependent Markovian vector Θ^Q are uncorrelated, have zero mean, unit variance. The size of these random displacements is connected to the mobility tensor via the fluctuation-dissipation theorem. The three decoupled equations of motion can be readily derived by replacing the generalized coordinate with the positions of the center of mass of the particles \mathbf{r} , their orientations \mathbf{q} and internal coordinates λ for translation, rotation [37] and internal states [12, 34], respectively.

IV. SIMULATION DETAILS

The properties of the particles were selected as in the original model to match experimental values as much as possible [12]. We focus on the central 30-90 segment of α -syn, which is key in driving phase transitions and fibrillization. Given that a protein in its disordered conformation is slightly more compact than a random coil of similar length, yet less compact than a tightly folded structure, we approximate the radius of gyration for the 30–90 segment as 2.61 nm. In the folded conformation, we approximate the length of a spherocylinder $L_R = 3.5$ nm as the average length of the five β -strands, inspired from solution NMR studies [40]. The diameter of a rod $D_R = 2.5$ nm was set as the average between the combined width of the five β -strands (≈ 4 nm) and the distance (≈ 1 nm) between two proteins along the fibril axis [12, 34]. To ensure that the transition between two different states is limited to a small window, we use $A_\mu = 10$. The depth of the double well potential was fixed at $\epsilon_\lambda^S = 3$ and $\epsilon_\lambda^R = 2$ for a disordered and an ordered protein, respectively. This choice is motivated by the fact that previous simulations have shown that these parameters are efficient in capturing different nucleation pathways as well as fibrillar growth [12, 34]. The radius of gyration of the modulator (≈ 1.43 nm) was chosen such that it corresponds to a typical radius of gyration of a folded polypeptide that is shorter in sequence than α -syn.

For the α -syn- α -syn interaction potentials, the parameters were selected to match the original model [12]. As such, the steepness of the attractive potential was fixed at $A_{\text{attr}} = 0.2 + 0.4 * (\mu_i + \mu_j)$, with A_{attr} in units of nm^{-1} . The parameters in Eq. (4) were chosen such that the relevant mechanisms in absence of any modulators are preserved, $\mathcal{C}_{\text{SS}} = 3$, $\mathcal{C}_{\text{SR}} = 0$, $\mathcal{C}_{\text{RR}}^{\text{W}} = 0$ and $\mathcal{C} = 20$. To understand the effects of the modulators, we varied the concentrations of added modulator, c_M , (0 to 32.5 μM) as well as their affinities towards the disordered and the ordered α -syn, \mathcal{C}_{MS} and \mathcal{C}_{MR} , respectively.

Simulation systems were initialized by placing 200 disordered ($\lambda = -2/3$) α -syn particles, with random positions and orientations and a variable number of modulators in a cubic simulation box with periodic boundary conditions. All simulations were carried out in implicit solvent, at the water viscosity of $\eta = 7 \cdot 10^{-4}$ Pa s, a temperature of 310 K and using a timestep $\Delta t = 1.3 \cdot 10^{-13}$ s for 52 μs per system. The mobility of the particles were calculated on the fly [12] and the internal mobility of the α -syn particles was fixed at $\mu^\lambda = 1.4 \cdot 10^{30}$ J/s, which ensures that transitions are rare events yet numerous transitions occur during a simulation.

V. RESULTS AND DISCUSSION

A. Modulator-independent phase transitions

To assess the effects of modulator concentration on α -synuclein assembly, 200 disordered proteins were placed in a cubic simulation box at a concentration of 150 μM and the modulator concentration, c_M , was systematically varied between 0 μM and 32.5 μM . In first instance, only repulsive in-

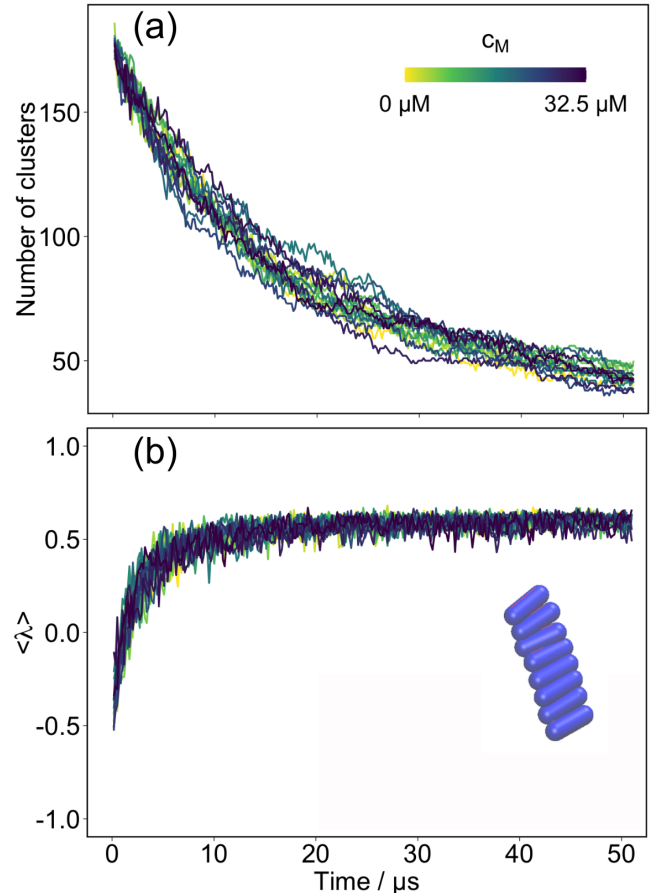


FIG. 2. Effects of repulsive modulators on α -syn clustering. (a) Number of clusters as a function of time at different modulator concentrations. (b) Time series of the average protein conformation in the simulation box at different modulator concentrations.

teractions between modulators and the protein were included, mimicking the effect of crowders in the semi-dilute regime [41]. The analysis focused on the temporal evolution of the number of clusters revealed a rapid decrease in the number of emerging clusters within the first few μs , which then levels toward a comparable number of clusters, independently of the modulator concentration (Fig. 2(a)). The profiles follow similar exponential decays aligning along the same averaged profile, and reach comparable cluster numbers (ca. 50), indicating that the modulator concentration has marginal impact on the aggregation kinetics. Simultaneously, the average internal conformation of the proteins, $\langle \lambda \rangle = \frac{1}{N} \sum_{i=1, N} \lambda_i$ over particles $i = 1..N$, shows an increase from ≈ -0.5 to $\approx +0.5$, corresponding to overall transitions from disordered to ordered states, respectively (Fig. 2(b)). In agreement with the cluster analysis, visual inspection indicates fibrillar structure formation across all systems, independent of repulsive modulator concentration (snapshot in Fig. 2(b)). Additionally, we find that fibril nucleation can occur both in one step as well as in two steps. More specific, multiple ordered proteins come into proximity and spontaneously assemble into a fibril nucleus (one-step nucleation), or nucleation can proceed via oligomer

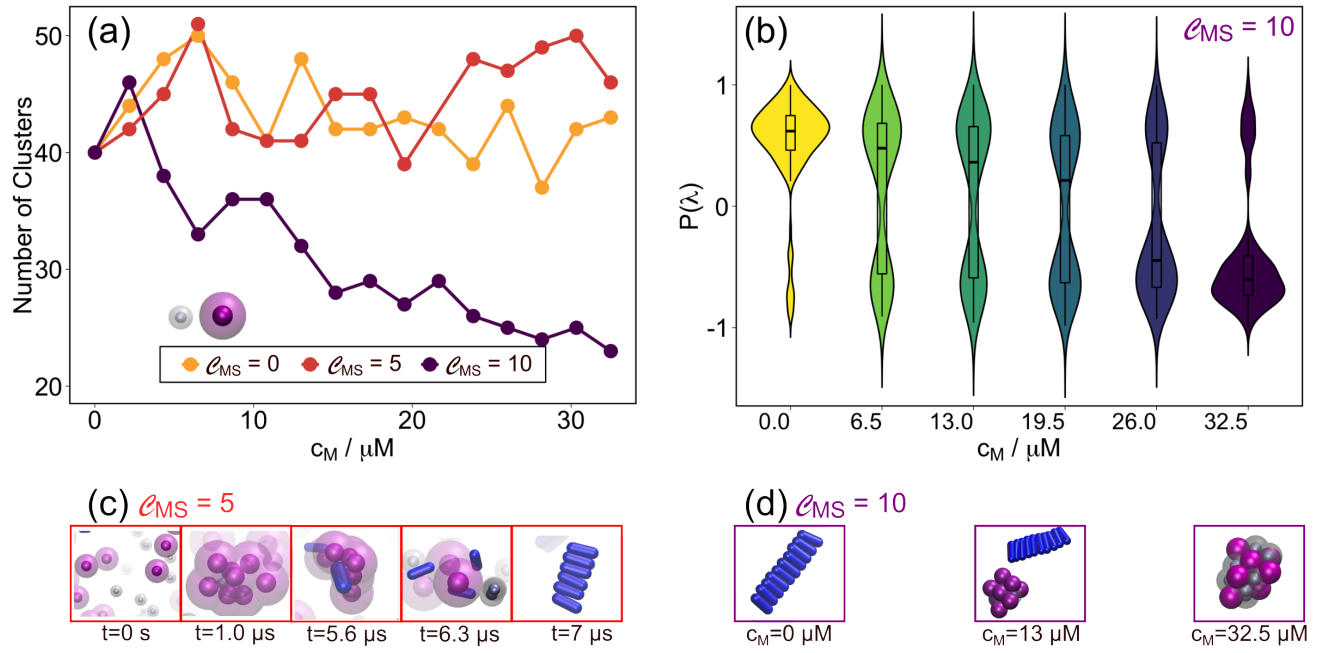


FIG. 3. Effects of modulator concentration and non-specific binding to the disordered protein. (a) Number of emerging clusters as a function of modulator concentration. (b) Violin plot of the protein conformations at high affinity of the modulators towards the disordered proteins. (c) Snapshots highlighting two-step nucleation at moderate modulator-protein attraction, $\mathcal{C}_{MS}=5$ and $c_M=32.5\ \mu M$. (d) Representative snapshots of the emerging structures at $c_M=0\ \mu M$, $c_M=13\ \mu M$ and $c_M=32.5\ \mu M$.

formation, followed by the conversion into growth-competent nuclei through structural rearrangement (two-step nucleation). While at low modulator concentrations, nucleation appears largely unchanged, at higher concentrations, visual inspection shows that the modulators can promote oligomer formation. The emerging oligomers either disintegrate, convert into fibrils or grow into larger assemblies. We ascribe this to the fact that modulators can effectively increase the local protein concentration, raising the probability of forming metastable clusters. Here, locally increased modulator concentrations can stabilize small oligomers just enough to extend their lifetimes before conversion or dissociation.

B. Nonspecific attraction tunes conformational ensembles and emerging species

Experiments have shown that non-specific agents can modulate α -synuclein dynamics and self-assembly [42, 43]. To investigate the effects of such agents, we endowed the modulators with isotropic attractions. To achieve this, we systematically varied the depth of the attractive well by modifying \mathcal{C}_{MS} from 0 to 10, thereby describing weak to strong binding towards the disordered protein. The analysis focused on the emerging protein cluster size indicates that, under purely repulsive modulation, the system yields ca. 40–50 aggregates independently of the modulator concentration (Fig. 3(a), yellow profile). A moderate attraction up to $5\ k_B T$ has marginal impact on the global cluster-size statistics, yielding a comparable number of clusters as in the case of repulsive modulators

(Fig. 3(a), orange profile). Further increase in attraction leads to a concentration-dependent decrease in number of emerging clusters. Specifically, increasing the modulator concentration leads to a decrease in the number of clusters from ca. 40 to ca. 20 for $0\ \mu M$ to $32.5\ \mu M$, respectively (Fig. 3(a), purple profile).

To probe the extent to which the nucleation pathways are modified, we zoomed in on the two-step nucleation mechanism for medium attraction of the modulator toward the disordered proteins at high modulator concentration (Fig. 3(c)). Within the first microsecond, multiple disordered proteins coalesce into a dynamic cluster. Subsequently, over the next $4\ \mu s$, the fluid-like assembly remains largely intact. A subset of proteins reorganize and adopt β -rich conformations, which then engage in cooperative association to result a fibrillar structure. Compared with previous results under identical conditions [12] in absence of modulators, the nucleation kinetics is slower, which increases the duration of the lag phase.

To investigate the structure of the emerging clusters at high attraction, we analyzed the protein conformations relying on the internal parameter λ . The violin plots in Fig. 3(b) show the distributions of the protein conformations at high attraction ($\approx 10\ k_B T$) between the modulator and the disordered proteins. The results show that at modulator concentrations below $6.5\ \mu M$, the system is mainly populated by β -rich proteins ($\lambda > 0$), which indicates that the formed clusters correspond primarily to fibrillar structures. As modulator concentration is increased ($\leq 26\ \mu M$), the λ -distribution gradually shifts towards disordered species as well ($\lambda < 0$), indicating a coexistence of disordered and β -rich structures. At high mod-

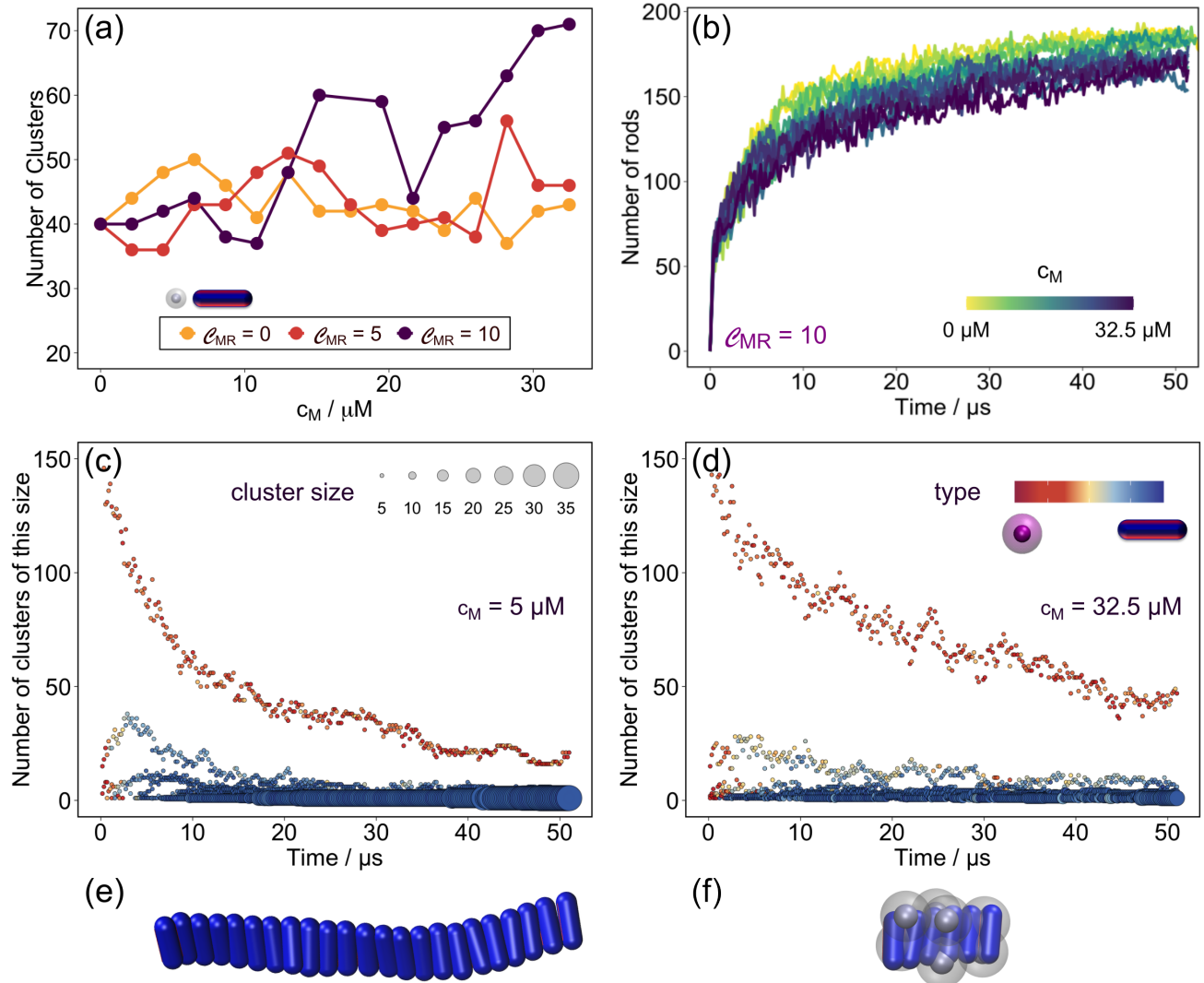


FIG. 4. Effects of β -specific modulators on α -syn fibrillization. (a) Number of protein clusters as a function of modulator concentration. (b) Time series of the number of β -rich proteins at different modulator concentrations and high modulator- β -rich protein affinity, $\mathcal{C}_{MR}=10$. (c-d) Time series of the type and size of the emerging clusters at $c_M=5\mu\text{M}$ and $c_M=32.5\mu\text{M}$, respectively. The symbol color encodes cluster type, *i.e.*, red for disordered, blue for β -rich and yellow for intermediate internal states, and symbol area encodes the cluster size. (e) Representative snapshot of an α -synuclein fibril at $c_M=5\mu\text{M}$ and (f) at $c_M=32.5\mu\text{M}$. At high modulator concentration the emerging fibrils are shorter due to the accumulation of modulators on the fibril surface thereby blocking incoming monomers to attach and continue fibrillar growth.

ulator concentrations ($32.5 \mu\text{M}$), the λ -distribution shows that the disordered state is favoured ($\lambda < 0$). In combination with the corresponding cluster size, this indicates the emergence of predominantly oligomeric species. Visual inspection of the simulations reveals that disordered proteins heteroassemble with modulators, which help stabilize the assembly (Movie S1, snapshots in Fig. 3(d)). This interaction promotes the progressive growth of the oligomer through monomer addition. The stabilized oligomer grows predominantly by stepwise monomer addition, rapidly exceeding the critical size of six monomers for conversion into a fibrillar nucleus [12], which inhibits the two-step nucleation mechanism.

All in all, our results indicate that nonspecific attraction towards the disordered state, equivalent to hydrophobic interactions, drives a concentration-dependent shift in the distribution of assembled species and modulates the kinetics of fibril nucleation.

C. β -selective modulators inhibit fibril elongation through surface "capping"

A therapeutically motivated strategy is to design binders that recognize β -rich conformations of α -synuclein and

thereby modulate fibril growth and seeding [44–46]. To understand the underlying mechanisms of such agents, we systematically varied the modulator affinity towards the β -rich conformations and investigated the effects on fibril nucleation and elongation.

The analysis focused on the number of clusters as a function of modulator concentration concentration, shows that at low to medium modulator- β -rich α -syn interactions, both the cluster count and their average internal state remain largely unchanged with increasing c_M , while the emerging species are predominantly β -rich (Fig. 4(a), Fig. S1). At higher affinity, the number of emerging clusters nearly doubles (from 40 to 70) in a dose-dependent manner at modulator concentrations over $12.5 \mu\text{M}$ (Fig. 4(a), purple line). Although the final products are primarily fibrillar independently of c_M (Fig. S1), the kinetics of the process is affected by the modulator concentration (Fig. S2). Specifically, tracking the time evolution of β -rich proteins reveals a rapid increase in the total number of rods within the first $10 \mu\text{s}$, reflecting the fast conversion of disordered proteins into ordered species, ascribed to fibril nucleation (Fig. 4(b)). This growth then levels off into a plateau, consistent with the establishment of a steady population of β -rich proteins. Comparing systems without modulators to those with modulators reveals that, while the onset of nucleation is marginally affected, the subsequent increase in rod number proceeds slower with increasing c_M (Fig. 4(b)).

Zooming in on the type and sizes of the emerging clusters shows that all systems transition from many small disordered clusters at early times (red symbols in Fig. 4(d-e)) to a few larger β -rich clusters at late times (blue symbols in Fig. 4(d-e)). At low modulator concentration, disordered proteins accumulate into clusters up to ten monomers within the first $\approx 5 \mu\text{s}$ (red symbols in Fig. 4(c)). A fraction converts directly to β -rich fibrils (red \rightarrow blue), while other clusters first form mixed intermediates (red \rightarrow yellow) and undergo structural rearrangements before maturing into β -rich structures (yellow \rightarrow blue). As the modulator concentration is increased, the size of the emerging clusters decreases (smaller blue symbol size in Fig. 4(d) as compared to the larger blue symbols in Fig. 4(c)). Specifically, at $c_M=32.5 \mu\text{M}$ in the first $10 \mu\text{s}$ small clusters consisting of both β -rich and disordered proteins form (Fig. 4(d)). Many of these evolve into fibrillar structures with less than 20 monomers in their composition, which persist until the end of the simulation. Relative to systems with fewer modulators, this corresponds to a significant reduction fibril length, *i.e.*, at $c_M=5 \mu\text{M}$, fibrils reach lengths of about 35 proteins (Fig. 4(c)), whereas at $c_M=32.5 \mu\text{M}$ they extend only up to roughly 20 proteins. Interestingly, modulator-coated fibril surfaces can occasionally bridge adjacent fibrils, facilitating lateral association and bundle formation. Additionally, the population of free, uncomplexed disordered proteins increases with modulator concentration (red symbols in Fig. 4(d-e)).

All in all, our results show that the α -syn proteins, which convert into β -rich conformations present high affinity surfaces for the modulators. These proteins can associate to form fibrils, which themselves act as attractive scaffolds for the modulators. As such the modulators can accumulate on the fibril surface. At sufficiently high modulator concentrations,

the adsorbed modulators act as surface “cappers” by forming a protective coating that can sterically or energetically prevent further incorporation of monomers, thereby inhibiting fibril elongation (Movie M2). This hypothesis is further supported by the increased population of free, disordered proteins at high modulator concentration, which indicates that monomers remain in solution rather than being sequestered into growing fibrils.

VI. DISCUSSION

More than 50 million people worldwide are affected by neurodegenerative disorders, such as Parkinson’s disease. The underlying disease mechanisms are linked to phase transitions of the protein α -synuclein, an intrinsically disordered protein also known as *protein chameleon* [47]. α -synuclein can undergo phase transitions giving rise to a wide spectrum of emergent species, ranging from liquid-like condensates and oligomers to β -rich fibrils. To understand the emergence of these species and the effects of molecular modulators on their formation mechanisms and kinetics, we performed coarse-grained simulations of α -synuclein [12, 34] in the presence of modulators. In this model, the protein is represented as a single, polymorphic particle that switches between a soft, isotropically interacting sphere representing the disordered state and an elongated spherocylinder with directional, hydrogen-bond-like attractions representing the β -rich state. The modulator is modeled as a single soft sphere with isotropic interactions representing a small peptide. Throughout our simulations, we systematically varied modulator concentration (0 – $32.5 \mu\text{M}$) along with its relative affinity (0 – $10 k_B T$) towards disordered versus ordered, β -rich states. Our results show that modulator concentration and interactions reshape the kinetic and thermodynamic pathways of α -syn self-assembly, fibril nucleation and elongation. The results are three-fold.

First, soft repulsive modulators act as as low-dose crowders that do not alter the formation of fibrils nor change the underlying mechanisms. Hence, fibril nucleation occurs both in one-step and in two-steps via dynamic disordered intermediates, and both mechanisms persist across different modulator concentrations. Our results are consistent with experiments showing the formation of fibrillar species also when in solution with different crowding agents (proteins, polysaccharides and polyethylene glycols) [48, 49]. While these experiments show a strong acceleration of fibrillation in presence of crowding agents, our simulations show marginal influence on the aggregation mechanisms when increasing the concentration to $32.5 \mu\text{M}$. This is most likely because we are in the semi-dilute regime, significantly below concentrations commonly used experimentally, where crowding is at least tenfold higher [48, 49].

Second, our results show that when modulators target disordered α -synuclein, they can embed within nascent oligomers to result in dynamic, liquid-like heteroassemblies (Fig. 3(d)). At intermediate modulator concentrations, disordered protein assemblies persist over extended periods before converting to

fibrils, consistent with a longer lag phase prior to fibril conversion. These findings align with experiments using the 4554W peptide, showing delayed aggregation via selective inhibition of primary nucleation, which extends the lag phase while leaving latter growth largely unaffected [50]. Increased affinity towards the disordered protein, further favors the stabilization of disordered, dynamically exchanging clusters, which continue to sequester monomers and modulators from solution. In this regime, one-step nucleation becomes the predominant fibrilization pathway. Although one-step nucleation is faster than two-step-nucleation, sequestration of monomers within large, disordered assemblies reduces the available free protein, limiting the monomers available for fibril growth. Mechanistically, these pathways align with the engineered β -wrapin AS69 activation, which binds monomeric α -synuclein and was shown to slow fibril elongation and block conversion of oligomeric precursors [51]. Furthermore, our results align with experiments showing that the antimicrobial peptide LL-III interacts with α -synuclein monomers and condensates to stabilize protein droplets and suppress conversion to the fibrillar state [52].

Third, β -selective modulators limit the growth of fibrillar structures by preventing free monomers to attach to the fibril tips and continue fibrillar growth. Generally, fibrillar growth proceeds via a dock-lock-mechanism, in which free monomers first attach to the preformed fibril (*dock*) and undergo structural rearrangements before they attain the fibril structure (*lock*) and give rise to a new growth-competent surface [17, 34, 53–59]. At coarser resolution, this is known as stop-and-go, a mechanism in which periods of active fibril elongation via monomer addition (*go*) are interrupted by extended pauses in elongation (*stop*) [34, 35, 60–64]. Our results show that modulators targeting β -rich states bind to the fibril surface, including the fibril ends, thereby sterically disfavoring the docking of incoming proteins. This essentially stabilizes and extends the *stop* phase of fibrillar growth. Our results provide mechanistic insight into experimentally designed peptides targeting β -rich fibrillar surfaces that coat the fibril surface with tunable stoichiometry [65] or stabilize the elongation-incompetent blocked state [66]. Additionally, our results show that modulators bridge between fibrils to form bundles of shorter fibrils with altered interfaces. As such, they fundamentally change the fibril seeding properties, providing a mechanistic explanation for experimental observations that bundled fibrils bridged by high-affinity peptides designed from the α -synuclein NAC core display reduced seeding ability compared to individual short fibrils [44].

VII. CONCLUSIONS AND PERSPECTIVES

We performed coarse-grained Brownian dynamics simulations to understand how modulators with distinct interaction profiles reshape α -synuclein phase transitions. Our results reveal a concentration- and affinity-dependent landscape in which non-specific modulators stabilize dynamic, liquid-like heteroassemblies of disordered species, extending the lag phase and suppressing nucleation, while β -selective modulators accumulated on fibril surfaces, yielding shorter fibrils oc-

asionally bundled with reduced elongation ability.

These simulations go beyond experimental observations to provide mechanistic insight by connecting modulator properties (affinity, concentration) to outcomes (nucleation, fibril length, bundling), which may be exploited in context of the development of novel therapeutic intervention strategies [67] and guide additional experimental testing. For instance, protein sequestration within disordered heteroassemblies can suppress fibril nucleation. As such, the rational design of peptides, rich in hydrophobic residues developed to bind in the non-amyloidogenic component of α -synuclein, could stabilize intermediate species to delay or even prevent fibril formation. Alternatively, structure-guided design of β -selective peptides with constrained backbones (via di-sulfide bonds or non-natural residues) can enable polymorph-specific recognition of cross- β architectures, achieving high-affinity fibril-end blocking (via hydrogen-bonding capabilities). Additionally, multivalent peptide conjugates linking two such β -selective constrained peptides can simultaneously occupy adjacent fibril surfaces and bridge fibrils laterally, resulting in bundled architecture, whose clearance can be compared against long, individual fibrils. Extending beyond α -synuclein, the generic nature of the model allows the extension to other polypeptides sharing the same emerging properties by adjusting geometrical parameters or introducing system-specific interactions, applicable to pathological (e.g. amyloid- β , TDP-43) and non-pathological functional polypeptides (e.g. silk or oat peptides). Such a framework can therefore inform the design of new nanomaterials with tunable and adaptable properties. For instance, engineering stimulus-responsive materials that use modulator-controlled fibril association in response to environmental triggers (e.g. pH, light, modulator concentration etc.) to dynamically tune mechanical properties or engineering nanostructures that control the interaction with surfaces [68–74].

ACKNOWLEDGMENTS

I.M.I. acknowledges support from the Sectorplan Bèta & Techniek of the Dutch Government and the Dementia Research - Synapsis Foundation Switzerland.

[1] C. B. Lücking and A. Brice, Alpha-synuclein and parkinson's disease, *Cell. Mol. Life Sci.* **57**, 1894–1908 (2000).

[2] I. N. Serratos, E. Hernández-Pérez, C. Campos, M. Aschner, and A. Santamaría, An update on the critical role of α -synuclein in parkinson's disease and other synucleinopathies: from tissue to cellular and molecular levels, *Mol. Neurobiol.* **59**, 620–642 (2021).

[3] M. G. Spillantini, M. L. Schmidt, V. M.-Y. Lee, J. Q. Trojanowski, R. Jakes, and M. Goedert, α -synuclein in lewy bodies, *Nature* **388**, 839–840 (1997).

[4] M. H. Polymeropoulos, C. Lavedan, E. Leroy, S. E. Ide, A. Dehejia, A. Dutra, B. Pike, H. Root, J. Rubenstein, R. Boyer, E. S. Stenroos, S. Chandrasekharappa, A. Athanasiadou, T. Papapetropoulos, W. G. Johnson, A. M. Lazzarini, R. C. Duvoisin, G. Di Iorio, L. I. Golbe, and R. L. Nussbaum, Mutation in the α -synuclein gene identified in families with parkinson's disease, *Science* **276**, 2045–2047 (1997).

[5] M. Goedert, Alpha-synuclein and neurodegenerative diseases, *Nat. Rev. Neurosci.* **2**, 492–501 (2001).

[6] L. Maroteaux, J. Campanelli, and R. Scheller, Synuclein: a neuron-specific protein localized to the nucleus and presynaptic nerve terminal, *J. Neurosci.* **8**, 2804–2815 (1988).

[7] P. H. Weinreb, W. Zhen, A. W. Poon, K. A. Conway, and P. T. Lansbury, Nacp, a protein implicated in alzheimer's disease and learning, is natively unfolded, *Biochem. J.* **35**, 13709–13715 (1996).

[8] R. Jakes, M. G. Spillantini, and M. Goedert, Identification of two distinct synucleins from human brain, *FEBS Lett.* **345**, 27–32 (1994).

[9] S. Mukherjee, A. Sakunthala, L. Gadhe, M. Poudyal, A. S. Sawner, P. Kadu, and S. K. Maji, Liquid-liquid phase separation of α -synuclein: A new mechanistic insight for α -synuclein aggregation associated with parkinson's disease pathogenesis, *J. Molec. Biol.* **435**, 167713 (2023).

[10] S. J. Wood, J. Wypych, S. Steavenson, J.-C. Louis, M. Citron, and A. L. Biere, α -synuclein fibrillogenesis is nucleation-dependent, *J. Biol. Chem.* **274**, 19509–19512 (1999).

[11] A. M. Morris, M. A. Watzky, and R. G. Finke, Protein aggregation kinetics, mechanism, and curve-fitting: A review of the literature, *Biochim. et Biophys. Acta - Proteins Proteom.* **1794**, 375–397 (2009).

[12] I. M. Ilie, W. K. den Otter, and W. J. Briels, A coarse grained protein model with internal degrees of freedom. application to α -synuclein aggregation, *J. Chem. Phys.* **144**, 10.1063/1.4942115 (2016).

[13] C. W. Shults, Lewy bodies, *Proc. Nat. Acad. Sci.* **103**, 1661–1668 (2006).

[14] W. Peelaerts, L. Bousset, A. Van der Perren, A. Moskalyuk, R. Pulizzi, M. Giugliano, C. Van den Haute, R. Melki, and V. Baekelandt, α -synuclein strains cause distinct synucleinopathies after local and systemic administration, *Nature* **522**, 340–344 (2015).

[15] M. S. Terakawa, Y. Lin, M. Kinoshita, S. Kanemura, D. Itoh, T. Sugiki, M. Okumura, A. Ramamoorthy, and Y.-H. Lee, Impact of membrane curvature on amyloid aggregation, *Biochim. et Biophys. Acta - Biomembr.* **1860**, 1741–1764 (2018).

[16] A. Rawat, R. Langen, and J. Varkey, Membranes as modulators of amyloid protein misfolding and target of toxicity, *Biochim. et Biophys. Acta - Biomembr.* **1860**, 1863–1875 (2018).

[17] I. M. Ilie and A. Caflisch, Simulation studies of amyloidogenic polypeptides and their aggregates, *Chem. Rev.* **119**, 6956–6993 (2019).

[18] B. Morel and F. Conejero-Lara, Early mechanisms of amyloid fibril nucleation in model and disease-related proteins, *Biochim. et Biophys. Acta - Proteins Proteom.* **1867**, 140264 (2019).

[19] Z. Yang, Y. Yao, Y. Zhou, X. Li, Y. Tang, and G. Wei, Egcg attenuates α -synuclein protofibril-membrane interactions and disrupts the protofibril, *Int. J. Biol. Macromol.* **230**, 123194 (2023).

[20] V. Oliveri, Toward the discovery and development of effective modulators of α -synuclein amyloid aggregation, *Eur. J. Med. Chem.* **167**, 10–36 (2019).

[21] S. K. Singh, A. Dutta, and G. Modi, α -synuclein aggregation modulation: An emerging approach for the treatment of parkinson's disease, *Future Med. Chem.* **9**, 1039–1053 (2017).

[22] K. Sivanesham, A. Byrne, M. Bisaglia, L. Bubacco, and N. Andersen, Binding interactions of agents that alter α -synuclein aggregation, *RSC Advances* **5**, 11577–11590 (2015).

[23] A. Mitra and N. Sarkar, Sequence and structure-based peptides as potent amyloid inhibitors: A review, *Archives Biochem. and Biophys.* **695**, 108614 (2020).

[24] R. L. Redler, D. Shirvanyants, O. Dagliyan, F. Ding, D. N. Kim, P. Kota, E. A. Proctor, S. Ramachandran, A. Tandon, and N. V. Dokholyan, Computational approaches to understanding protein aggregation in neurodegeneration, *J. Molec. Cell Biol.* **6**, 104–115 (2014).

[25] D. S. Davidson, A. M. Brown, and J. A. Lemkul, Insights into stabilizing forces in amyloid fibrils of differing sizes from polarizable molecular dynamics simulations, *J. Molec. Biol.* **430**, 3819–3834 (2018).

[26] G. Chakraborty, A. Chaudhary, and N. Patra, Dual allosteric and orthosteric inhibition of 14-3-3 ζ - α -synuclein interaction: A multiscale simulation and machine learning approach, *Adv. Theor. Simul.* (2025).

[27] P. Robustelli, A. Ibanez-de Opakua, C. Campbell-Bezat, F. Giordanetto, S. Becker, M. Zweckstetter, A. C. Pan, and D. E. Shaw, Molecular basis of small-molecule binding to α -synuclein, *J. Am. Chem. Soc.* **144**, 2501–2510 (2022).

[28] T. T. Ali, M. Merghani, M. Al-Azzani, L. M. Gatzemeier, M. Hoppert, D. Kaloyanova, T. F. Outeiro, P. Neumann, B. Popova, and G. H. Braus, Rationally designed peptides inhibit the formation of α -synuclein fibrils and oligomers, *Eur. J. Med. Chem.* **289**, 117452 (2025).

[29] V. Tozzini, Multiscale modeling of proteins, *Acc. Chem. Res.* **43**, 220–230 (2009).

[30] C. Wu and J.-E. Shea, Coarse-grained models for protein aggregation, *Curr. Op. Struc. Biol.* **21**, 209–220 (2011).

[31] A. Wasim, S. Menon, and J. Mondal, Modulation of α -synuclein aggregation amid diverse environmental perturbation, *eLife* **13** (2024).

[32] G. Tesei and K. Lindorff-Larsen, Improved predictions of phase behaviour of intrinsically disordered proteins by tuning the interaction range, *Open Research Europe* **2**, 94 (2023).

[33] A. S. Rauh, G. Tesei, and K. Lindorff-Larsen, A coarse-grained model for disordered proteins under crowded conditions, *Protein Sci.* **34** (2025).

[34] I. M. Ilie, W. K. den Otter, and W. J. Briels, The attachment of α -synuclein to a fiber: A coarse-grain approach, *J. Chem. Phys.* **146**, 115102 (2017).

[35] M. M. Wördehoff, O. Bannach, H. Shaykhaliyahu, A. Kulawik, S. Schiefer, D. Willbold, W. Hoyer, and E. Birkmann, Sin-

gle fibril growth kinetics of α -synuclein, *J. Molec. Biol.* **427**, 1428–1435 (2015).

[36] C. Vega and S. Lago, A fast algorithm to evaluate the shortest distance between rods., *Computers and Chemistry* **18**, 55 (1994).

[37] I. M. Ilie, W. J. Briels, and W. K. den Otter, An elementary singularity-free rotational brownian dynamics algorithm for anisotropic particles, *J. Chem. Phys.* **142**, 114103 (2015).

[38] H. C. Öttinger, *Stochastic processes in polymeric fluids* (Springer, 1996).

[39] C. W. Gardiner, *Handbook of stochastic methods for physics, chemistry and the natural sciences*, 3rd ed., Springer Series in Synergetics, Vol. 13 (Springer-Verlag, Berlin, 2004) pp. xviii+415.

[40] M. Vilar, H.-T. Chou, T. Lührs, S. K. Maji, D. Riek-Lohr, R. Verel, G. Manning, H. Stahlberg, and R. Riek, The fold of α -synuclein fibrils, *Proc. Nat. Acad. Sci.* **105**, 8637 (2008).

[41] A. Bhattacharya, Y. C. Kim, and J. Mittal, Protein–protein interactions in a crowded environment, *Biophysical Reviews* **5**, 99–108 (2013).

[42] S. Heravi, J. V. D. Power, A. Yethiraj, and V. Booth, The effects of biological crowders on fibrillization, structure, diffusion, and conformational dynamics of α -synuclein, *Protein Science* **33** (2024).

[43] W. P. Lipiński, B. S. Visser, I. Robu, M. A. A. Fakhree, S. Lindhoud, M. M. A. E. Claessens, and E. Spruijt, Biomolecular condensates can both accelerate and suppress aggregation of α -synuclein, *Science Advances* **8** (2022).

[44] S. Sangwan, S. Sahay, K. A. Murray, S. Morgan, E. L. Guenther, L. Jiang, C. K. Williams, H. V. Vinters, M. Goedert, and D. S. Eisenberg, Inhibition of synucleinopathic seeding by rationally designed inhibitors, *eLife* **9** (2020).

[45] L. C. Hjelm, W. Paslawski, C. Lendel, S. F. Svedmark, P. Svenningsson, S. Ståhl, H. Lindberg, and J. Löfblom, Engineered sequestrins inhibit aggregation of pathogenic alpha-synuclein mutants, *Frontiers in Immunology* **16** (2025).

[46] T. T. Ali, M. Merghani, M. Al-Azzani, L. M. Gatzemeier, M. Hoppert, D. Kaloyanova, T. F. Outeiro, P. Neumann, B. Popova, and G. H. Braus, Rationally designed peptides inhibit the formation of α -synuclein fibrils and oligomers, *European Journal of Medicinal Chemistry* **289**, 117452 (2025).

[47] V. N. Uversky, J. Li, and A. L. Fink, Evidence for a partially folded intermediate in α -synuclein fibril formation, *J. Biol. Chem.* **276**, 10737 (2001).

[48] V. N. Uversky, E. M. Cooper, K. S. Bower, J. Li, and A. L. Fink, Accelerated α -synuclein fibrillation in crowded milieu, *FEBS Letters* **515**, 99–103 (2002).

[49] I. Horvath, R. Kumar, and P. Wittung-Stafshede, Macromolecular crowding modulates α -synuclein amyloid fiber growth, *Biophys. J.* **120**, 3374–3381 (2021).

[50] R. M. Meade, K. J. Morris, K. J. Watt, R. J. Williams, and J. M. Mason, The library derived 4554w peptide inhibits primary nucleation of α -synuclein, *J. Molec. Biol.* **432**, 166706 (2020).

[51] E. D. Agerschou, P. Flagmeier, T. Saridaki, C. Galvagnion, D. Komnig, L. Heid, V. Prasad, H. Shaykhalishahi, D. Willbold, C. M. Dobson, A. Voigt, B. Falkenburger, W. Hoyer, and A. K. Buell, An engineered monomer binding-protein for α -synuclein efficiently inhibits the proliferation of amyloid fibrils, *eLife* **8** (2019).

[52] R. Oliva, S. K. Mukherjee, L. Ostermeier, L. A. Pazurek, S. Kriegler, V. Bader, D. Prumbaum, S. Raunser, K. F. Winklhofer, J. Tatzelt, and R. Winter, Remodeling of the fibrillation pathway of α -synuclein by interaction with antimicrobial peptide II-iii, *Chemistry – A European Journal* **27**, 11845–11851 (2021).

[53] M. Schor, A. S. J. S. Mey, F. Noe, and C. E. MacPhee, Sheding light on the dock-lock mechanism in amyloid fibril growth using markov state models, *J. Phys. Chem. Lett.* **6**, 1076 (2015).

[54] M. Schor, J. Vreede, and P. G. Bolhuis, Elucidating the locking mechanism of peptides onto growing amyloid fibrils through transition path sampling, *Biophys. J.* **103**, 1296 (2012).

[55] I. M. Ilie, D. Nayar, W. K. den Otter, N. F. A. van der Vegt, and W. J. Briels, Intrinsic Conformational Preferences and Interactions in α -Synuclein Fibrils: Insights from Molecular Dynamics Simulations, *J. Chem. Theor. Comp.* **14**, 3298 (2018).

[56] S. Jalali, R. Zhang, M. P. Haataja, and C. L. Dias, Nucleation and growth of amyloid fibrils, *J. Phys. Chem. B* **127**, 9759–9770 (2023).

[57] P. H. Nguyen, M. S. Li, G. Stock, J. E. Straub, and D. Thirumalai, Monomer adds to preformed structured oligomers of $\alpha\beta$ -peptides by a two-stage dock-lock mechanism, *Proc. Nat. Acad. Sci.* **104**, 111 (2007).

[58] G. Reddy, J. E. Straub, and D. Thirumalai, Dynamics of locking of peptides onto growing amyloid fibrils, *Proc. Nat. Acad. Sci.* **106**, 11948 (2009).

[59] J. E. Straub and D. Thirumalai, Toward a molecular theory of early and late events in monomer to amyloid fibril formation, *Annu. Rev. Phys. Chem.* **62**, 437 (2011).

[60] T. Ban, K. Yamaguchi, and Y. Goto, Direct observation of amyloid fibril growth, propagation, and adaptation, *Acc. Chem. Res.* **39**, 663 (2006).

[61] J. Ferkinghoff-Borg, J. Fonslet, C. B. Andersen, S. Krishna, S. Pigoletti, H. Yagi, Y. Goto, D. Otzen, and M. H. Jensen, Stop-and-go kinetics in amyloid fibrillation, *Phys. Rev. E* **82**, 010901 (2010).

[62] W. Hoyer, D. Cherny, V. Subramaniam, and T. M. Jovin, Rapid self-assembly of α -synuclein observed by *in situ* atomic force microscopy, *J. Molec. Biol.* **340**, 127 (2004).

[63] T. Ban, M. Hoshino, S. Takahashi, D. Hamada, K. Hasegawa, H. Naiki, and Y. Goto, Direct observation of $\alpha\beta$ amyloid fibril growth and inhibition, *J. Molec. Biol.* **344**, 757 (2004).

[64] D. Pinotsi, A. K. Buell, C. Galvagnion, C. M. Dobson, G. S. Kaminski Schierle, and C. F. Kaminski, Direct observation of heterogeneous amyloid fibril growth kinetics via two-color super-resolution microscopy, *Nanolett.* **14**, 339 (2014).

[65] S. Bismut, M. M. Schneider, M. Miyasaki, Y. Feng, E. J. Wilde, M. D. Gunawardena, T. P. J. Knowles, G. S. Kaminski Schierle, L. S. Itzhaki, and J. R. Kumita, Using a stable protein scaffold to display peptides that bind to alpha-synuclein fibrils, *Protein Sci.* **34** (2025).

[66] C. M. Schulz, A. Pfister, and W. Hoyer, Fibril core regions in engineered α -synuclein dimer are crucial for blocking of fibril elongation, *Biochim. et Biophys. Acta - Adv.* **4**, 100110 (2023).

[67] D. de Raffele and I. M. Ilie, Unlocking novel therapies: cyclic peptide design for amyloidogenic targets through synergies of experiments, simulations, and machine learning, *Chem. Comm.* **60**, 632 (2024).

[68] Y. Han, Y. Cao, J. Zhou, Y. Yao, X. Wu, S. Bolisetty, M. Diner, S. Handschin, C. Lu, and R. Mezzenga, Interfacial electrostatic self-assembly of amyloid fibrils into multifunctional protein films, *Advanced Science* **10** (2023).

[69] J. W. Smith, X. Jiang, H. An, A. M. Barclay, G. Licari, E. Tajkhorshid, E. G. Moore, C. M. Rienstra, J. S. Moore, and Q. Chen, Polymer-peptide conjugates convert amyloid into protein nanobundles through fragmentation and lateral association, *ACS Applied Nano Materials* **3**, 937–945 (2019).

[70] M. A. N. Soliman, A. Khedr, T. Sahota, R. Armitage, R. Allan, K. Laird, N. Allcock, F. I. Ghuloum, M. H. Amer, R. Alazragi,

C. J. C. Edwards-Gayle, J. K. Wychowaniec, A. V. Vargiu, and M. A. Elsawy, Unraveling the atomistic mechanism of electrostatic lateral association of peptide β -sheet structures and its role in nanofiber growth and hydrogelation, *Small* **21** (2025).

[71] M. Paesani and I. M. Ilie, Metaparticles: Computationally engineered nanomaterials with tunable and responsive properties, *J. Chem. Phys.* **161**, 244905 (2024).

[72] M. Paesani and I. M. Ilie, Physical mechanisms of nanoparticle-membrane interactions: A coarse-grained study, *bioRxiv* (2025).

[73] W. Wang, B. He, T. Xiao, M. Xu, B. Liu, Y. Gao, Y. Chen, J. Li, B. Ge, J. Ma, and H. Ge, Bioinspired amyloid fibril-based hydrogel with engineering programmable functionalities for diverse applications, *Adva. Fun. Mat.* **33** (2023).

[74] X. Shao, C. Yan, C. Wang, C. Wang, Y. Cao, Y. Zhou, P. Guan, X. Hu, W. Zhu, and S. Ding, Advanced nanomaterials for modulating alzheimer's related amyloid aggregation, *Nanoscale Advances* **5**, 46–80 (2023).